van der Waals Screening by Single-Layer Graphene and Molybdenum Disulfide

Stanislav Tsoi,*,† Pratibha Dev,‡ Adam L. Friedman,§ Rory Stine,⊥ Jeremy T. Robinson,‡ Thomas L. Reinecke,‡ and Paul E. Sheehan†

†Chemistry Division, ‡Electronic Science and Technology Division, and §Materials Division, US Naval Research Laboratory, Washington, D.C. 20375, United States and ⊥NOVA Research, Alexandria, Virginia 22308, United States

ABSTRACT A sharp tip of atomic force microscope is employed to probe van der Waals forces of a silicon oxide substrate with adhered graphene. Experimental results obtained in the range of distances from 3 to 20 nm indicate that single-, double-, and triple-layer graphenes screen the van der Waals forces of the substrate. Fluorination of graphene, which makes it electrically insulating, lifts the screening in the single-layer graphene. The van der Waals force from graphene determined per layer decreases with the number of layers. In addition, increased hole doping of graphene increases the force. Finally, we also demonstrate screening of the van der Waals forces of the silicon oxide substrate by single- and double-layer molybdenum disulfide.

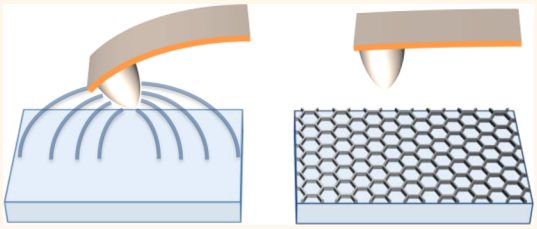

KEYWORDS: graphene · van der Waals interactions · screening · atomic force microscopy

Since its first experimental realization, most graphene research has focused on its striking 2D physics and its superlative physical properties, such as high electron mobility, record thermal conductivity, impressive mechanical strength, *etc.*[1,2] Almost from the beginning, however, another aspect of graphene has been recognized as truly unprecedented: graphene was the first atomically thin, crystalline material.[2] From the perspective of surface science, this opened an equally unprecedented opportunity, since graphene could be applied to an existing surface in a conformal fashion allowing one to modify surfaces one atomic layer at a time. A number of experiments have demonstrated the dramatic effects such modification could have on surface properties. Addition of graphene and indeed other monolayer materials, such as hexagonal boron nitride and molybdenum disulfide (MoS_2), to silicon oxide drastically reduced nanoscale friction.[3] A single graphene layer on top of a copper surface completely prevented its oxidation by the ambient.[4] In turn, the chemical reactivity of graphene was shown to be affected strongly by the supporting substrate.[5] Recently, sequential assembly of monolayer materials into complex van der Waals heterogeneous stacks was demonstrated,[6] extending further the opportunity to modify surfaces at the single atomic layer level.

Surface energy is a property determined by nanometer scale interactions, such as van der Waals (vdW) interactions and hydrogen bonding, and so may be significantly modified by the addition of the monolayer materials. A recent series of experiments made a first attempt to assess the effect of graphene on the surface energy of various substrates using the water contact angle measurement. Unfortunately, this simple technique has led to a range of contradictory results for the same substrate, from no effect,[7] to an intermediate effect,[8] to a strong effect.[9] Because graphene was not expected to form strong hydrogen bonds, each of those results was attributed to a different way the addition of graphene affected the vdW interactions of the substrate, leading to a current controversy.

A close examination reveals the limited utility of the contact angle measurement for studying the vdW forces, principally because it does not exploit the strong

* Address correspondence to: stanislav.tsoi@nrl.navy.mil.

Received for review September 9, 2014 and accepted November 20, 2014.

Published online November 20, 2014
10.1021/nn5050905

dependence of the surface forces on the separation between the interacting bodies. Consequently, in the present work, we employ a sharp tip of an atomic force microscope (AFM) to probe the vdW forces of a graphene-coated SiO_2 substrate at different distances from the substrate. This approach enables us to uncover an unprecedented physical phenomenon: atomically thin graphene completely screens the vdW forces of the SiO_2 substrate, with all surface interactions being confined to the graphene layer only. Further, because the measured force is due to graphene only, we explore unimpeded its dependence on the number of graphene layers and its doping. A similar, strong vdW screening of the SiO_2 substrate by MoS_2 is also shown. Thus, we demonstrate the unique effect of the monolayer materials on the surface vdW forces, constituting a novel method to shape and control the surface energy.

RESULTS AND DISCUSSION

To obtain the cleanest possible graphene samples we used micromechanical cleavage[10,11] of graphene on top of the 275 nm thick SiO_2 layer, which produces flakes of a few-micron square area (Figure 1A). Areas of the exposed substrate and those covered by graphene with varying numbers of layers can be readily identified in the AFM image. Once the image is recorded, the AFM tip can be positioned over an area of interest and the force, F, as a function of separation, d, probed (Figure 1B). Note that areas covered with single-layer, double-layer, and triple-layer graphenes here have a typical lateral size of 1 μm, *i.e.*, too small for the contact angle measurement.[7−9] However, because the lateral dimensions of the tip asperity are only of order 10 nm, vdW measurements on a sample with a particular number of layers can be unambiguously carried out.

Figure 1C exhibits typical $F(d)$ dependences recorded over a SiO_2 substrate covered with single-, double-, and triple-layer graphenes; similar dependences obtained on another graphene flake are provided in Figure S1 (Supporting Information). The data points for each region in Figure 1C are averages over 100 individual scans recorded sequentially over the same spot. All data were obtained with the same Si_3N_4 AFM tip. In addition, a $F(d)$ dependence probed with the same tip on a separate, highly ordered pyrolytic graphite (HOPG) sample is included in Figure 1. In the context of the substrate-supported graphene, HOPG can be considered as a sample with an infinite number of graphene layers.

The AFM tip experiences attractive force from all samples investigated as evidenced by the negative values of the measured force. The attraction strengthens monotonically as the tip approaches the sample such that at separations <3 nm (<2 nm for HOPG) the attraction overwhelms the cantilever bending causing it to snap into contact with the sample surface.[12]

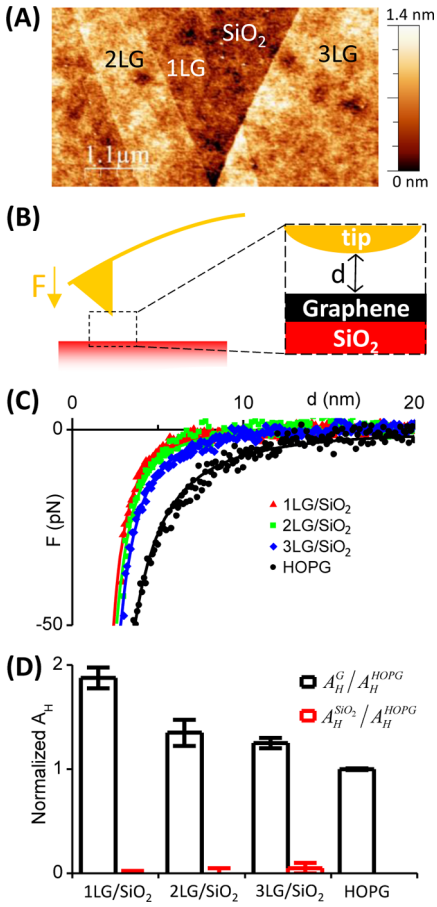

Figure 1. (A) AFM topography image of graphene exfoliated on top of a SiO_2 substrate showing areas covered by varying number of graphene layers. 1LG = single-layer graphene, 2LG = double-layer graphene, 3LG = triple-layer graphene. (B) Schematic representation of the AFM force−separation measurement. Force F exerted on the tip by the sample is measured as a function of their separation d. (C) The $F(d)$ dependence measured over areas covered by different number of graphene layers. Dots are experimental data, lines fits. In addition, the $F(d)$ dependence measured with the same tip over a separate HOPG sample is included. (D) Hamaker coefficients determined from the fits for graphene and the underlying SiO_2 and normalized relative to HOPG.

Consequently, only data above this snap-in range are retained for analysis. As shown in Figure 1C, the interaction between the tip and sample is weakest when the sample is SiO_2 covered with single-layer graphene. Additional layers of graphene strengthen the interaction, while the interaction of the tip with HOPG is significantly stronger than with any of the graphene-coated SiO_2 samples.

The range of separations investigated limits observed interactions to the vdW forces. For vdW interactions between the AFM tip and a homogeneous half space such as HOPG, a few assumptions within a standard dielectric continuum model lead to a simple analytical expression for $F(d)$. The first assumption, based on the rapid decay of vdW interactions with distance, asserts that the vdW forces are mostly applied to the asperity of the tip.[13] Further, the asperity is

assumed to be spherical with a radius of curvature R (Figure 1B). Adopting the Derjaguin approximation for a vdW interaction between a sphere and the half space, an expression for small separations ($d \ll R$) is obtained[13,14]

$$F = -\frac{A_H R}{6d^2} \quad (1)$$

where A_H is a material coefficient, known as a Hamaker coefficient, characterizing interaction strength between a unit volume of material of the tip and a unit volume of material of the half space. A fit to the HOPG data using eq 1 and treating $A_H R$ as a single parameter is included in Figure 1C as a solid black line. It provides a good approximation to the data suggesting overall validity of the assumptions leading to eq 1.

To interpret the heterogeneous samples, such as SiO_2 covered with graphene, eq 1 needs to be extended. A simplifying approximation of pairwise interactions is often adopted, in which the net force on the AFM tip is the sum of its separate interactions with graphene and the SiO_2 substrate.[13] This approximation is not always justified within a rigorous Lifshitz theory of vdW interactions[13] but does lead to more intuitive physical interpretation. Working under the pairwise interaction approximation, eq 1 is modified for the heterogeneous sample to yield

$$F = -\frac{A_H^G R}{6d^2} + \frac{A_H^G R}{6(d+t)^2} - \frac{A_H^{SiO_2} R}{6(d+t)^2} \quad (2)$$

where A_H^G and $A_H^{SiO_2}$ are Hamaker coefficients for interaction of the tip with graphene and the SiO_2 substrate, respectively, and t the thickness of the graphene layer. Note that d is measured from the top surface of the graphene layer. In this form, the first two terms on the right-hand side of eq 2 describe interaction of the tip with the graphene layer and the last term that with the SiO_2 substrate.

Fits to the experimental data obtained with eq 2 are shown as solid lines in Figure 1C. To avoid overparameterizing the fits the thickness t for the single-, double-, and triple-layer graphenes was set to be corresponding multiples of the interlayer separation in graphite (0.34 nm), while $A_H^G R$ and $A_H^{SiO_2} R$ treated as the fitting parameters. The obtained parameters are summarized in Table 1. Remarkably, all the fits yield negligibly small $A_H^{SiO_2} R$ suggesting effective screening of the vdW interaction between the Si_3N_4 tip and SiO_2 substrate by the single-, double-, or triple-layer graphene. While it was not possible to measure direct vdW interaction between the Si_3N_4 tip and SiO_2 substrate due to the presence of surface water on the hydrophilic SiO_2 surface, further experimental data presented in this work demonstrate that it is not intrinsically negligible. Therefore, atomically thin few-layer graphene appears effectively opaque to vdW forces.

The AFM tip positioned over the graphene-covered SiO_2 substrate experiences attraction from graphene only, as if it were a freely suspended membrane. In this manner, the $F(d)$ dependences in Figure 1C exhibit a progression in vdW interaction strength as graphene layers are added one by one, starting from a single layer and ending with the bulk (HOPG). Beyond the fits, Figure 1C shows this graphically in that the probe must approach to within 7 nm of the graphene-covered SiO_2 sample to detect a force, while only needing to approach within 15 nm above HOPG. This is because in the former the forces sum only over the single to few layers of graphene, while in the latter the summation is over the homogeneous half-space.

While a rigorous theoretical treatment of the vdW screening by graphene is beyond the scope of the present work, several qualitative supporting arguments can be considered. Among the three contributions to vdW forces—Keesom orientation, Debye induction, and London dispersion interactions—the last is usually the strongest originating from correlated quantum mechanical oscillations of dipoles in the interacting bodies.[13] The correlation is facilitated by the dipole−dipole interaction, and an intervening body such as graphene can screen electric field lines of the interacting dipoles, thus disrupting the correlation and effectively screening the interaction. Graphene, with its semimetallic electronic band structure, offers charge carriers (electrons and holes) which can rearrange spatially to screen external electric fields. Indeed, theoretical calculations predict that even intrinsic, undoped graphene can strongly screen the electrostatic field of a nearby charge.[15] Doping of graphene enhances its screening capacity and leads to a complete screening of the external charge as expected of a metallic material.[15] Experimental data obtained with Raman scattering and Kelvin probe force microscopy (KFM) on the present graphene samples (see the Supporting Information) indicate that they are modestly hole-doped. Estimates based on the Raman scattering suggest the doping level of 5×10^{12} holes/cm^2 in the single-layer graphene. It is natural to extend the argument of the electrostatic screening of graphene from the London dispersion contribution to the Keesom orientation and Debye induction contributions which are also mediated by the dipole−dipole interaction.

The London dispersion interaction, however, does not occur in the electrostatic regime but at finite frequencies. The most important contributions result from frequency ranges corresponding to optical absorption in the interacting bodies. For dielectrics, such as the SiO_2 substrate and Si_3N_4 tip, these typically lie below 3×10^{15} s^{-1} (ref 14). A theoretical study shows that in both undoped and doped graphene, the charge carriers will rearrange to cancel a suddenly created electric field on a time scale of 0.26 fs, corresponding to a period of the $\sigma+\pi$ plasmon oscillation; i.e. with a time

TABLE 1. Fitting Parameters Determined from the $F(d)$ Dependences of a Si_3N_4 Tip Interacting with Graphene-Covered SiO_2 and Corresponding Hamaker Coefficients Reported Relative to That of the Si_3N_4 Tip Interacting with HOPG

	t^a (nm)	$A_H^G R$ (10^{-27} J·m)	$A_H^{SiO_2} R$ (10^{-27} J·m)	$A_H^{HOPG} R$ (10^{-27} J·m)	A_H^G/A_H^{HOPG}	$A_H^{SiO_2}/A_H^{HOPG}$
1LG/SiO_2	0.34	7.5 ± 0.4	0.0 ± 0.1		1.875 ± 0.100	0.000 ± 0.025
2LG/SiO_2	0.68	5.4 ± 0.5	0.0 ± 0.2		1.350 ± 0.125	0.000 ± 0.050
3LG/SiO_2	1.02	5.0 ± 0.2	0.2 ± 0.2		1.250 ± 0.050	0.050 ± 0.050
HOPG				4.00 ± 0.03		

[a] t is the thickness of the graphene layer.

constant around 4×10^{15} s^{-1} (ref 15). Thus, it appears that the carriers in graphene are sufficiently fast to screen the electrodynamic vdW interactions of the tip and substrate.

Because the same probe was used for each set of experiments, we can extract the relative strengths of the Hamaker coefficient from the $A_H R$ values (Table 1 and Figure 1D). The obtained ratios A_H^G/A_H^{HOPG} suggest that the strength of the vdW interaction per layer monotonically decreases with the number of the layers tending to the interaction strength of HOPG.[16] Such a trend is not unexpected because vdW interactions depend on electronic polarizabilities of the interacting bodies[13] and therefore their band structure. The last is known to change dramatically from the linear dispersion in the single-layer to quadratic in the double-layer graphene.[17] Additional graphene layers should further shift the band structure toward that of graphite. A recent study of graphene adhesion to SiO_2 demonstrated a 50% stronger adhesion of the single-layer graphene than the two- to five-layer graphenes.[18] That result is qualitatively in agreement with our Hamaker coefficients because adhesion should be dominated by the vdW interaction of the SiO_2 substrate with the closest, bottom layer of the multilayer graphene. On the basis of the present Hamaker coefficients (Figure 1D), such an interaction will be strongest for the single-layer graphene, drop significantly for the double-layer graphene, and monotonically decrease for graphenes with more layers. It will be interesting to see if future theoretical calculations can reproduce the stronger Hamaker coefficient from the fewer layer graphenes.

If single-layer graphene is opaque to vdW interactions and this opacity is related to its semimetallic nature and mobile charge carriers, then atomically thin materials of semiconducting and insulating character, when substituted for graphene, may prove partially or fully transparent to the vdW interactions. Fluorination is an efficient method of turning graphene into an insulator.[19,20] To test the above hypothesis, we fluorinated exfoliated graphene by exposure to XeF_2 gas and probed the vdW properties of SiO_2 covered with the fluorinated graphene.

Figure 2A shows an AFM topography image of a graphene flake exfoliated on SiO_2 and subsequently treated with XeF_2. The original flake (see Figure S3,

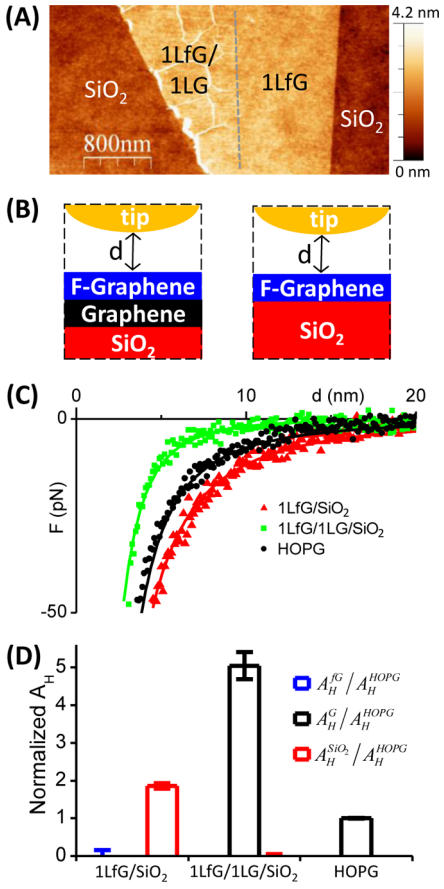

Figure 2. (A) AFM topography image of graphene exfoliated on top of a SiO_2 substrate and treated with XeF_2 gas. 1LfG designates single-layer fluorinated graphene, 1LfG/1LG a double layer consisting of a top fluorinated graphene and underlying graphene. The gray dashed line denotes a boundary between 1LfG and 1LfG/1LG (B) Schematic representation of the AFM force measurement carried over 1LfG/SiO_2 (right) and 1LfG/1LG/SiO_2 (left). (C) Representative $F(d)$ dependences measured with a Si_3N_4 AFM tip over 1LfG/SiO_2, 1LfG/1LG/SiO_2, and a separate HOPG. Dots are experimental data, lines fits. (D) Hamaker coefficients determined from the fits for the fluorinated graphene, underlying graphene and SiO_2 and normalized relative to HOPG.

Supporting Information) contained both single- and double-layer regions. Under the current conditions, fluorination occurs only on the top surface to approximately 20−25% coverage[19,20] such that, for the double-layer graphene, the top layer is fluorinated and the bottom layer remains pristine. Subsequent lattice mismatch and stress between the layers (within the double-layer region) leads to numerous wrinkles seen

TABLE 2. Fitting Parameters Determined from the $F(d)$ Dependences of a Si_3N_4 Tip Interacting with SiO_2 Covered with Fluorinated Graphene and Corresponding Hamaker Coefficients Reported Relative to That of the Si_3N_4 Tip Interacting with HOPG[a]

	t_G (nm)	t_{fG} (nm)	$A_H^{fG}R$ (10^{-27} J·m)	$A_H^{G}R$ (10^{-27} J·m)	$A_H^{SiO_2}R$ (10^{-27} J·m)	A_H^{fG}/A_H^{HOPG}	A_H^{G}/A_H^{HOPG}	$A_H^{SiO_2}/A_H^{HOPG}$
1LfG/SiO_2		0.80	0.0 ± 0.7		8.2 ± 0.3	0.00 ± 0.16		1.86 ± 0.07
1LG/1LfG/SiO_2	0.34	0.80	0	22.2 ± 1.6	0.0 ± 0.2	0	5.05 ± 0.36	0.00 ± 0.05

[a] $A_H^{HOPG}R = (4.40 \pm 0.04) \times 10^{-27}$ J·m. t_{fG} and t_G are thicknesses of the fluorinated and underlying graphenes, respectively.

in the image. The extent of the fluorination was explored using Raman scattering and KFM (Supporting Information). Raman spectra recorded over the single- and double-layer parts of the flake exhibit significant departure from corresponding spectra of pristine single- and double-layer graphenes. KFM images show strong charging of the fluorinated graphene, with a polarity opposite to that of the pristine graphene. Together these data indicate strong fluorination of the exposed graphene surface.

The $F(d)$ dependence was probed over the fluorinated graphene (1LfG/SiO_2), over a 1LfG/1LG/SiO_2 stack, and over a HOPG reference (Figure 2C). Additional dependences recorded at other parts of the sample are given in Figure S4 (Supporting Information). The interaction recorded over 1LfG/SiO_2 shows dramatic evolution compared to its prefluorinated, pristine state (1LG/SiO_2 in Figure 1C). A detectable force develops already at long separations (d > 15 nm) and the shape of the dependence resembles that over HOPG (homogeneous half-space), suggesting a significant contribution from the SiO_2 substrate. A fit using eq 2 shows that the interaction is dominated by SiO_2 with only a negligible contribution from the fluorinated graphene (see Figure 2D and Table 2). Thus, whereas semimetallic graphene screens the vdW forces, the insulating fluorinated graphene exhibits a partial to full transparency.

In contrast, $F(d)$ determined over the 1LfG/1LG/SiO_2 stack still exhibits the vdW opacity, with the tip needing to approach within 10 nm to detect a force. Even though the top fluorinated layer has become transparent to vdW forces, the bottom layer remains pristine and can screen the vdW interactions (Figure 2B). Our density functional theory calculations of the electronic structure in the stack support the concept of two separate layers, the top insulating fluorinated and bottom pristine graphenes (Supporting Information). Fitting these data requires extension of eq 2 to include the two atomically thin layers as well as the SiO_2 half-space

$$F = -\frac{A_H^{fG}R}{6d^2} + \frac{A_H^{fG}R}{6(d+t_{fG})^2} - \frac{A_H^{G}R}{6(d+t_{fG})^2} + \frac{A_H^{G}R}{6(d+t_{fG}+t_G)^2} - \frac{A_H^{SiO_2}R}{6(d+t_{fG}+t_G)^2} \quad (3)$$

where A_H^{fG} is the Hamaker coefficient for interaction of the Si_3N_4 tip with the fluorinated graphene and t_{fG} (t_G) the thickness of the fluorinated (pristine) graphene. In practice, however, such an approach leads to overparameterization because the separation d is significantly greater than thickness of the layers t_{fG} (t_G). To simplify the fitting, we use the previous result showing no contribution from the fluorinated layer to set $A_H^{fG} = 0$. The thickness of the fluorinated graphene cannot be obtained directly from the AFM measurements because the XeF_2 treatment slightly etches exposed SiO_2 areas adjacent to the flakes (Figure 2A). In our recent work, we showed that graphene nanoribbons reduced in fluorinated graphene by scanning probe lithography appear thinner than the surrounding fluorinated graphene by about 0.5 nm,[21] therefore we assume here $t_{fG} = t_G + 0.5\ \text{nm} \approx 0.80$ nm. A fit with these values using eq 3 reveals no contribution from SiO_2 ($A_H^{SiO_2} R = 0$, see Figure 2D and Table 2) showing that the pristine bottom layer continues to screen the vdW forces of the substrate. Taken together, the results obtained on pristine (Figure 1) and fluorinated graphene (Figure 2) provide a strong case for the vdW screening by graphene.

Normalizing the Hamaker coefficients to that of HOPG reveals significantly enhanced interaction from the pristine layer in the 1LfG/1LG/SiO_2 stack compared to single-layer graphene; compare A_H^G/A_H^{HOPG} in Table 2 (5.05 ± 0.36) with that in Table 1 (1.875 ± 0.100). Even if we allow non-zero $A_H^{fG} R$ in the fit, the former A_H^G/A_H^{HOPG} will still come out noticeably greater than the latter. We attribute this increased vdW interaction to the doping of the bottom graphene layer by the overlying fluorinated graphene. 3D metals exhibit significantly stronger vdW interactions than 3D dielectrics due to a high polarizability associated with their collective electronic modes, *i.e.*, plasmons.[14] The semimetallic nature of graphene allows dramatic changes in its doping, between electrons and holes to concentrations as high as 10^{13} carriers/cm^2 (ref 1). Experimental and theoretical studies indicate that this can lead to significant changes in the plasmon dispersion and electronic polarizability.[22,23] Consequently, numerical calculations find that increased doping produces stronger vdW interaction between two graphene sheets, as well as between a graphene sheet and a SiO_2 half-space.[24] Recent electronic transport measurements from our group demonstrated that fluorinated graphene adjacent to a graphene nanoribbon acted as a strong acceptor increasing hole concentration in the latter.[25] Thus, in the present 1LfG/1LG/SiO_2 stack electron

transfer from the bottom pristine layer to the top fluorinated layer increases hole doping of the former. Raman scattering and KFM support this assertion and suggest a doping level >2 × 10^{13} holes/cm^2 in the pristine layer of the 1LfG/1LG/SiO_2 stack compared to 5 × 10^{12} holes/cm^2 in the single-layer graphene (Supporting Information). Thus, increased doping appears to strengthen the vdW interactions of graphene. We also note that the thickness-dependence of the Hamaker coefficient seen in Figure 1D may partially stem from doping.

Because graphene exhibits such a rich vdW behavior, it is natural to extend investigation of vdW properties to other monolayer materials. Single-layer MoS_2, a semiconductor with a direct band gap ~1.8 eV,[26] differs from both the semimetallic graphene and insulating but noncrystalline fluorinated graphene; therefore, in the present study we explore vdW properties of MoS_2 prepared by micromechanical cleavage. Figure 3A shows a MoS_2 flake exfoliated on a SiO_2 substrate featuring single- and double-layer areas. Occasionally, flakes with thickness greater than 6−7 nm can be found on the same substrate (Figure S6, Supporting Information); these are used as bulk MoS_2.

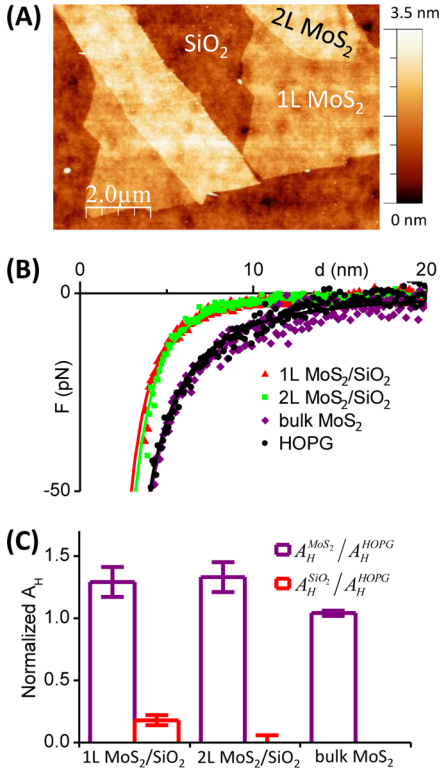

Figure 3. (A) AFM topography image of MoS_2 exfoliated on top of a SiO_2 substrate. 1L MoS_2 = single-layer MoS_2, 2L MoS_2 = double-layer MoS_2. (B) Representative *F*(*d*) dependences measured with a Si_3N_4 AFM tip over SiO_2 substrate covered with single-layer, double-layer, and bulk MoS_2. A reference *F*(*d*) dependence recorded with the same tip over HOPG is also included. Dots are experimental data, lines fits. (C) Hamaker coefficients determined from the fits for MoS_2 and SiO_2 and normalized relative to HOPG.

Figure 3B demonstrates typical *F*(*d*) dependences measured with a Si_3N_4 AFM tip over a SiO_2 substrate covered with single- and double-layer MoS_2 as well as a thick (bulk) MoS_2 flake. The latter can be readily fitted with eq 1 justifying the assumption that the thick MoS_2 flakes exhibit bulk vdW behavior. For reference, a *F*(*d*) dependence measured with the same tip on a separate HOPG sample is also included in Figure 3B. Coincidently, HOPG and bulk MoS_2 appear to possess vdW interactions of very similar strength. The dependences recorded over SiO_2 covered with single- and double-layer MoS_2 display a close similarity to those over graphene-covered SiO_2 suggesting strong screening of the vdW interactions by few-layer MoS_2. Fits using eq 2 and assuming *t* equal to multiple of the interlayer separation in bulk MoS_2 (0.615 nm) yield strong, albeit incomplete, screening by the single-layer MoS_2 and even stronger, perhaps complete, screening by the double-layer MoS_2. Hamaker coefficients deduced from the fits are summarized in Figure 3C and Table 3.

The strong vdW screening by the semiconducting single-layer MoS_2 may seem unexpected at first. We note, however, that exfoliation of MoS_2 on SiO_2 often leads to its doping.[11] Transfer characteristics of a MoS_2 field-effect transistor exhibit zero conductivity at a negative back-gate potential suggesting heavy electron doping.[27] A recent KFM measurement shows negative charging of exfoliated MoS_2 relative to the supporting SiO_2 also consistent with electron doping.[28] It is possible that the observed strong screening is aided by the presence of electrons and associated plasmon polarizability in MoS_2. The same electronic polarizability of plasmons may also be responsible for the greater Hamaker coefficients in the single- and double-layer MoS_2 compared to presumably undoped (or less doped) bulk MoS_2 (Figure 3C). In addition, the evolution of the electronic band structure of MoS_2, from that of direct band gap with value of 1.8 eV in the single-layer MoS_2 to that of indirect band gap with value of 1.2 eV in bulk,[26]

TABLE 3. Fitting Parameters Determined from the *F*(*d*) Dependences of a Si_3N_4 Tip Interacting with SiO_2 Covered with MoS_2 and Corresponding Hamaker Coefficients Reported Relative to That of the Si_3N_4 Tip Interacting with HOPG

	t (nm)	$A_H^{SiO_2}$ *R* (10^{-27} J·m)	$A_H^{MoS_2}$ *R* (10^{-27} J·m)	A_H^{HOPG} *R* (10^{-27} J·m)	$A_H^{SiO_2}/A_H^{HOPG}$	$A_H^{MoS_2}/A_H^{HOPG}$
1L MoS_2/SiO_2	0.62	0.9 ± 0.2	6.3 ± 0.6		0.18 ± 0.04	1.29 ± 0.12
2L MoS_2/SiO_2	1.23	0.0 ± 0.3	6.5 ± 0.5		0.00 ± 0.06	1.33 ± 0.10
bulk MoS_2			5.1 ± 0.1			1.04 ± 0.02
HOPG				4.9 ± 0.1		

may contribute to the observed difference in the Hamaker coefficients.

CONCLUSION

In conclusion, the obtained experimental results reveal a new physical phenomenon: the vdW screening by few-layer graphene and MoS_2. The screening enables isolation and direct measurement of the vdW forces from the monolayer materials. In this manner, the vdW force per layer from the few-layer graphene is shown to decrease in strength with each added layer and in the single-layer graphene become stronger with its doping. Because vdW forces are always present in graphene samples and devices, the uncovered properties have a fundamental implication. For example, they may explain how graphene adhesion to the substrate occurs, a critical consideration in the context of graphene nanomechanical devices.[29] They may also influence how micromechanical cleavage of 2D atomic crystals occurs. Consider, for example, the typical yield of single-, double-, and multilayer flakes. Lastly, these properties may play a critical role in the self-assembly of the vdW heterostructures, where the monolayer materials are added sequentially on top of each other starting with a supporting 3D substrate.[6]

A second, more applied, implication is that adding a single atomic heterogeneous layer to a solid substrate can dramatically modify its surface interactions. With several stable 2D materials already available and an ability to combine them into the vdW heterostructures, this opens an opportunity for bottom-up surface energy engineering. The possibilities for tailoring surface interactions are further expanded by the ability to dope 2D materials in situ using the electrical gating, which should allow continuous tuning of their vdW strength.

METHODS

Graphene and MoS_2 samples were prepared on Si substrates with a 275 nm thick SiO_2 layer using the micromechanical cleavage technique.[10,11] Flakes exfoliated on top of SiO_2 were identified in an optical microscope. Fluorination of graphene was accomplished by exposure of the exfoliated graphene samples to XeF_2 gas using a Xactix etching system. The system was used in pulse mode and samples were exposed to 5 cycles with $P(XeF_2)$ = 1 Torr, $P(N_2)$ = 35 Torr, and pulse time = 60 s (5 min total exposure time). After preparation, all samples were stored inside a class 100 clean room in a cabinet under nitrogen atmosphere. Immediately prior to AFM force measurements, the samples were annealed in a rapid thermal annealer (RTA) under vacuum (residual pressure $\sim 10^{-5}$ Torr) at 200 °C for the duration from 60 to 90 min to remove inadvertent organic contamination.

All force measurements were taken within a few days after preparation. This was especially important for the fluorinated samples because degradation of the top, fluorinated layer could be detected in AFM images 2 weeks after preparation. While the fluorinated graphene had been treated in RTA twice by that time, it is not clear if the degradation was spontaneous or induced by the annealing. In contrast, unmodified graphene and MoS_2 could undergo several RTA treatments and did not show signs of deterioration for at least 6 months.

AFM measurements were carried out on Asylum Cypher AFM equipped with an environmental chamber. During the measurements, nitrogen atmosphere with residual oxygen content below 0.2% was maintained inside the chamber. This should be compared to 23% oxygen content in ambient and indicative of greatly reduced humidity. Soft rectangular Si_3N_4 cantilevers (Asylum Research RC800PSA) employed in the measurements were cleaned in piranha solution immediately prior to each measurement. The piranha solution was prepared by mixing concentrated sulfuric acid (>98%) and 30% hydrogen peroxide in a ratio of 3:1. (Caution: piranha solution produces a highly exothermic oxidizing reaction when exposed to organic compounds). The cantilever was dipped in the piranha solution for 3 min and then thoroughly washed in deionized water and air-dried.

The measurement started with recording an AFM image of the sample area containing exfoliated flakes in the contact mode, from which areas of exposed SiO_2 as well as those covered with varying number of layers of graphene or MoS_2 could be identified. Next, the AFM tip was positioned over a spot of interest, *e.g.*, SiO_2 covered with single-layer graphene. Care was taken to choose the spot in the middle of the single-layer graphene, *i.e.*, away from the exposed SiO_2 and graphenes with other number of layers, to ensure that the tip interacts with the single-layer graphene only. One hundred force curves were recorded sequentially for subsequent averaging. The measurement was repeated at other spots of interest, *e.g.*, SiO_2 covered with double- and triple-layer graphene. After force measurements on graphene-covered SiO_2 samples, reference force measurements were carried out on freshly cleaved HOPG.

In measuring a force curve, the sample is brought toward the tip by a piezo scanner until the two are in contact (approach part of the force curve) and then the piezo movement is reversed and the sample taken away from the tip (retract part of the force curve). During the piezo scan, cantilever bending b caused by a force exerted on the tip by the sample is recorded as a function of the piezo position z for both approach and retract. Positive values of the bending correspond to the repulsive force and negative values to the attractive force. The reversal from the approach to retract is triggered by reaching a preset positive value of the bending corresponding to an applied force of approximately 1 nN. The recorded $b(z)$ dependences are converted into force dependences $F(d)$, where d is the separation between the tip and sample. The force is obtained by $F = kb$, where k is a predetermined spring constant of the cantilever. For explanation on a more involved derivation of d from the measured $b(z)$; see ref 30. Analysis of the contact mechanics realized in the present work (see the Supporting Information) shows that both the sample and the tip experience only elastic deformations during the experiment and that their net deformation is negligible compared to the deduced separations d, indicative of the infinitely hard contact.[30]

In this work, the z scan ranged from 40 nm for SiO_2 covered with graphene to 100 nm for HOPG. Each approach and retract part took 0.1 s. Slower scans led to appearance of low frequency noise in b, while faster scans did not appreciably reduce noise. The spring constant of the cantilevers (around 100 pN/nm) was determined experimentally using thermal noise calibration. Only $F(d)$ obtained on the approach contained information on the near range, attractive van der Waals (vdW) forces. The retract portion of the force curve was affected by the tip adhesion and snap-out instability, which prevented probing force at small d. The one hundred $F(d)$ individual dependences recorded sequentially over the same spot were averaged to yield the representative force dependence.

The present experimental scheme and fitting procedure yield $A_H R$. We chose not to measure R independently to avoid introducing an additional uncertainty in A_H. For $R \approx 40$ nm, determination of the tip shape with SEM or an inverse tip

imaging using sharp spikes may easily lead to a 20% uncertainty. Instead, $A_H^{HOPG}R$ measured with the same tip serves as a reference and $A_H^{G}R$ and $A_H^{SiO_2}R$ deduced from the fits are reported as ratios to $A_H^{HOPG}R$, thus eliminating unknown R. Such an approach also avoids an additional uncertainty in A_HR associated with measuring absolute values of F, which requires knowledge of k. Modern calibration procedures yield k with a realistic uncertainty around 10%. In taking the ratios $A_H^{SiO_2}/A_H^{HOPG}$ and A_H^{G}/A_H^{HOPG} the spring constant is effectively eliminated.

AFM images were processed with Nanotec WSXM freeware.[31]

Conflict of Interest: The authors declare no competing financial interest.

Supporting Information Available: Description of experimental procedures and calculations; additional experimental and calculation results. This material is available free of charge *via* the Internet at http://pubs.acs.org.

Acknowledgment. This work was supported by the Naval Research Laboratory Base Program. P.D. appreciates the support of the National Research Council through a National Research Council Fellowship. We thank Mr. David Zapotok for his assistance with fabrication procedures.

Note Added after ASAP Publication: This paper was published ASAP on December 4, 2014. The Supporting Information file was replaced and the revised version was reposted on December 8, 2014.

REFERENCES AND NOTES

1. Geim, A.; Novoselov, K. The Rise of Graphene. *Nat. Mater.* **2007**, *6*, 183–191.
2. Geim, A. Graphene: Status and Prospects. *Science* **2009**, *324*, 1530–1534.
3. Lee, C.; Li, Q.; Kalb, W.; Liu, X.; Berger, H.; Carpick, R.; Hone, J. Frictional Characteristics of Atomically Thin Sheets. *Science* **2010**, *328*, 76–80.
4. Chen, S.; Brown, L.; Levendorf, M.; Cai, W.; Ju, S.; Edgeworth, J.; Li, X.; Magnuson, C.; Velamakanni, A.; Piner, R.; *et al.* Oxidation Resistance of Graphene-Coated Cu and Cu/Ni Alloy. *ACS Nano* **2011**, *5*, 1321–1327.
5. Wang, Q.; Jin, Z.; Kim, K.; Hilmer, A.; Paulus, G.; Shih, C.; Ham, M.; Sanchez-Yamagishi, J.; Watanabe, K.; Taniguchi, T.; *et al.* Understanding and Controlling the Substrate Effect on Graphene Electron-Transfer Chemistry *via* Reactivity Imprint Lithography. *Nat. Chem.* **2012**, *4*, 724–732.
6. Geim, A.; Grigorieva, I. Van Der Waals Heterostructures. *Nature* **2013**, *499*, 419–425.
7. Rafiee, J.; Mi, X.; Gullapalli, H.; Thomas, A.; Yavari, F.; Shi, Y.; Ajayan, P.; Koratkar, N. Wetting Transparency of Graphene. *Nat. Mater.* **2012**, *11*, 217–222.
8. Shih, C.; Strano, M.; Blankschtein, D. Wetting Translucency of Graphene. *Nat. Mater.* **2013**, *12*, 866–869.
9. Raj, R.; Maroo, S.; Wang, E. Wettability of Graphene. *Nano Lett.* **2013**, *13*, 1509–1515.
10. Novoselov, K.; Geim, A.; Morozov, S.; Jiang, D.; Zhang, Y.; Dubonos, S.; Grigorieva, I.; Firsov, A. Electric Field Effect in Atomically Thin Carbon Films. *Science* **2004**, *306*, 666–669.
11. Novoselov, K.; Jiang, D.; Schedin, F.; Booth, T.; Khotkevich, V.; Morozov, S.; Geim, A. Two-Dimensional Atomic Crystals. *Proc. Natl. Acad. Sci. U.S.A.* **2005**, *102*, 10451–10453.
12. Ashby, P.; Chen, L.; Lieber, C. Probing Intermolecular Forces and Potentials with Magnetic Feedback Chemical Force Microscopy. *J. Am. Chem. Soc.* **2000**, *122*, 9467–9472.
13. Parsegian, V. A. *Van Der Waals Forces: A Handbook for Biologists, Chemists, Engineers, and Physicists*; Cambridge University Press: New York, 2006; p xv, 380 p.
14. Israelachvili, J. N. *Intermolecular and Surface Forces: with Applications to Colloidal and Biological Systems*, 2nd ed.; Academic Press: London, 1991; p xxi, 450 pp.
15. Despoja, V.; Mowbray, D.; Vlahovic, D.; Marusic, L. TDDFT Study of Time-Dependent and Static Screening in Graphene. *Phys. Rev. B* **2012**, *86*, 195429.
16. We note that the Hamaker coefficient is defined in the present work per unit volume. In this manner, each sheet in the double-layer graphene interacts weaker with the tip than the single-layer graphene; nevertheless, the two sheets of the double-layer graphene do combine to yield a stronger net interaction than the single-layer graphene (Figure 1C).
17. Das Sarma, S.; Adam, S.; Hwang, E.; Rossi, E. Electronic Transport in Two-Dimensional Graphene. *Rev. Mod. Phys.* **2011**, *83*, 407–470.
18. Koenig, S.; Boddeti, N.; Dunn, M.; Bunch, J. Ultrastrong Adhesion of Graphene Membranes. *Nat. Nanotechnol.* **2011**, *6*, 543–546.
19. Robinson, J.; Burgess, J.; Junkermeier, C.; Badescu, S.; Reinecke, T.; Perkins, F.; Zalalutdniov, M.; Baldwin, J.; Culbertson, J.; Sheehan, P.; *et al.* Properties of Fluorinated Graphene Films. *Nano Lett.* **2010**, *10*, 3001–3005.
20. Stine, R.; Lee, W.-K.; Whitener, K. E.; Robinson, J. T.; Sheehan, P. E. Chemical Stability of Graphene Fluoride Produced by Exposure to XeF_2. *Nano Lett.* **2013**, *13*, 4311–4316.
21. Lee, W.; Tsoi, S.; Whitener, K.; Stine, R.; Robinson, J.; Tobin, J.; Weerasinghe, A.; Sheehan, P.; Lyuksyutov, S. Robust Reduction of Graphene Fluoride Using an Electrostatically Biased Scanning Probe. *Nano Res.* **2013**, *6*, 767–774.
22. Grigorenko, A.; Polini, M.; Novoselov, K. Graphene Plasmonics. *Nat. Photonics* **2012**, *6*, 749–758.
23. Hwang, E.; Das Sarma, S. Dielectric Function, Screening, and Plasmons in Two-Dimensional Graphene. *Phys. Rev. B* **2007**, *75*, 205418.
24. Sarabadani, J.; Naji, A.; Asgari, R.; Podgornik, R. Many-Body Effects in the Van Der Waals-Casimir Interaction Between Graphene Layers. *Phys. Rev. B* **2011**, *84*, 155407.
25. Lee, W.; Robinson, J.; Gunlycke, D.; Stine, R.; Tamanaha, C.; King, W.; Sheehan, P. Chemically Isolated Graphene Nanoribbons Reversibly Formed in Fluorographene Using Polymer Nanowire Masks. *Nano Lett.* **2011**, *11*, 5461–5464.
26. Mak, K.; Lee, C.; Hone, J.; Shan, J.; Heinz, T. Atomically Thin MoS_2: A New Direct-Gap Semiconductor. *Phys. Rev. Lett.* **2010**, *105*, 136805.
27. Radisavljevic, B.; Radenovic, A.; Brivio, J.; Giacometti, V.; Kis, A. Single-Layer MoS_2 Transistors. *Nat. Nanotechnol* **2011**, *6*, 147–150.
28. Li, Y.; Xu, C.; Zhen, L. Surface Potential and Interlayer Screening Effects of Few-Layer MoS_2 Nanoflakes. *Appl. Phys. Lett.* **2013**, *102*, 143110.
29. Bunch, J.; Dunn, M. Adhesion Mechanics of Graphene Membranes. *Solid State Commun.* **2012**, *152*, 1359–1364.
30. Butt, H.; Cappella, B.; Kappl, M. Force Measurements with the Atomic Force Microscope: Technique, Interpretation and Applications. *Surf. Sci. Rep.* **2005**, *59*, 1–152.
31. Horcas, I.; Fernandez, R.; Gomez-Rodriguez, J.; Colchero, J.; Gomez-Herrero, J.; Baro, A., WSXM: A Software for Scanning Probe Microscopy and A Tool for Nanotechnology. *Rev. Sci. Instrum.* **2007**, *78*.